Polymer Chemistry

ROYAL SOCIETY OF CHEMISTRY

PAPER

View Article Online
View Journal | View Issue

Cite this: *Polym. Chem.*, 2023, **14**, 1213

Colorimetric 3D printable base-detectors exploiting halocromic core-substituted naphthalenediimides†

Beatrice Tosetto,[a,b] Matteo Gastaldi,[c,d,e] Giacomo Renno,[c,d,f] Candido Fabrizio Pirri,[a,g] Claudia Barolo, [c,d] Andrea Fin[c] and Ignazio Roppolo *[a,g]

3D printing field is in rapid evolution, and its applications are widening continuously. Among the different techniques available, light induced vat-methods are demonstrated to be particularly suitable for developing functional devices due to their superior precision and their high flexibility in terms of materials properties. An emerging strategy for imparting functional properties consists of the use of functional dyes, which can confer peculiar properties even at low contents, improving at the same time polymerization control and printing precision. Herein, an ad-hoc synthesized core-substituted naphthalene diimide (cNDIs) dye is investigated as a functional dye for Digital Light Processing 3D printing, to give pH sensitivity properties to complex objects. The employed cNDI shows multi-color responsivity towards different conditions, spanning from yellow to blue. Different 3D printable matrices are here compared, and among those poly(ethylene glycol) diacrylate is selected since it maximizes the dye response when in contact with acid/basic solutions, also showing good miscibility, fast photopolymerization kinetics, and excellent CAD fidelity of the 3D printed structures. Furthermore, it is also demonstrated that the 3D printed structures are responsive to basic vapors, as well as to organic solution containing Lewis bases. These results go far beyond standard use of pH-responsive dyes, opening up to new and wider applications. At last, stimuli-responsive 3D devices are fabricated, producing smart lab-ware and microfluidic devices which can give *in operando* visual responses towards basic vapors and basic organic solutions.

Received 23rd December 2022,
Accepted 19th February 2023

DOI: 10.1039/d2py01593e

rsc.li/polymers

Introduction

Additive Manufacturing (AM) and 3D printing (3DP) are predicted to revolutionize industrial production and everyday life in the next decades, enabling the production of devices with highly complex shapes, usually impossible to obtain through traditional production techniques.[1] In its early stages, most of the efforts in 3DP were focused on improving the equipment, optimizing models and software, and obtaining faster printing with higher resolution. Only recently, attention was devoted to the development of new 3D printable materials, aiming at gathering materials and design to achieve synergistic effects that cannot be obtained otherwise.[2,3] Among the different 3D printing technologies, Digital Light Processing (DLP) is particularly attractive since it can enable the fabrication of objects with excellent final resolutions, CAD fidelity, high complexity, fast printing process together with low costs and materials consumption.[4,5] Furthermore, since it is based on liquid photocurable formulations, it is easy to modify the printable materials to obtain tailored properties.[6–8] On the other hand, some drawbacks still limit the full development of DLP 3D printing, such as the impossibility of obtaining multi-material objects on the *XY*-plane, the reduced size of printable devices, and, most of all, the limited palette of available photocurable materials, which is still in growth.[9]

Photocurable formulations for DLP are basically composed of photocurable monomers/oligomers and a photoinitiator. While the formers determine the polymeric features (*i.e.*, mechanical, chemical, and surface properties), the latter is needed to start the polymerization process by absorbing the incident radiation. Furthermore, fillers, dyes, and other addi-

[a]*Department of Applied Science and Technology, Politecnico di Torino, Corso Duca degli Abruzzi 24, Torino 10129, Italy. E-mail: ignazio.roppolo@polito.it*
[b]*Department of Chemistry, Biology and Biotechnology, University of Perugia, Via Elce di Sotto 8, 06123 Perugia, Italy*
[c]*Department of Chemistry, University of Torino, Via Pietro Giuria 7, 10125 Torino, Italy*
[d]*NIS Interdepartmental Centre, University of Torino, Via Gioacchino 15/a, 10125 Torino, Italy*
[e]*GAME Lab, Department of Applied Science and Technology (DISAT), Politecnico di Torino, Torino 10129, Italy*
[f]*School of Chemistry and Biochemistry, University of Geneva, 30 quai Ernest Ansermet, 1211 Geneva, Switzerland*
[g]*Center for Sustainable Future Technologies, Italian Institute of Technology, Via Livorno 60, 10144 Turin, Italy*

† Electronic supplementary information (ESI) available. See DOI: https://doi.org/10.1039/d2py01593e

tives may be added.[10,11] Among those, dye is used to compete with the photoinitiator in the absorption of the light source used for 3D printing, slowing down the photopolymerization process and enabling a better space control of the reaction, which in turn improves the resolution.[11,12] As a side effect, the presence of dye usually leaves a final color which is often undesired or, in the best option, only used for aesthetic purposes.

Recently, new research approaches have been developed, aiming to exploit functional dyes to improve printing resolutions and to provide new specific properties to the material. In this frame, functional dyes were used in 3D printing to fabricate polymeric waveguides, devices with optically tunable mechanical properties, mechanochromic strain sensors, devices with photo-controlled gas permeability, and many more.[13,14]

In this work, the properties of core-substituted naphthalene diimide (cNDIs) dyes were exploited to develop base sensing 3D printed materials. cNDIs are versatile compounds able to span the whole visible spectrum upon simple structural modifications. Electron-donor groups in the core create a push–pull system with the imides moieties, shifting both absorption and emission profiles along the visible spectrum. In a complementary manner, imide substitution can finely tune solubility and supramolecular assembly without affecting the photophysical properties.[15–18] Herein, two hydroxyl groups have been inserted on the aromatic core, while the imide sites have been decorated with long octyl chains. As previous work on similar systems proved, the obtained dye (namely, NDI-OH) modulates the photophysical traits upon pH changes due to the two hydroxyl groups undergoing acid–base equilibria. While two deprotonated groups move the absorption in the deep-red region of the visible spectrum, their bis-protonated analogue is hypsochromically shifted to *ca.* 460 nm. Summarizing, NDI-OH color varies from yellow to its complementary blue/purple color. This provides good sensitivity also for necked human eyes.[19]

Due to these remarkable properties, NDI-OH was thus used as responsive dye to fabricate polymeric 3D printed colorimetric sensors for bases, able to detect both liquid and vapor phases. Colorimetric devices are usually based on dispersed dyes in different matrices, such as polymers, silica gel, glass, or paper.[20] The device's final properties and efficiency depend mainly on three factors: (i) the selected materials, (ii) their interaction with sensed species, and (iii) the design optimization.[20,21] On the other hand, the select hosting matrix should not hinder the adsorption of sensed species and their diffusion into the sensor's inner parts.[21] In fact, the colorimetric response time is strongly related to the total time requested by the target species to complete those steps. For these reasons, the device's design optimization becomes crucial, to reduce the involved material thickness and ensure device integrity;[20] in this context 3D printing can play a key-role.

Furthermore, dyes' leaching from the polymeric matrix represents a great limitation, that can affect the stability and durability of the device as well as the color homogeneity and sensitivity.[22,23] To solve those problems, long alkyl chains were grafted on NDI-OH dye, to improve miscibility, and homogeneity and to avoid leaching.

After preliminary investigations on the most suitable matrix, NDI-OH has been embedded in PEGDA-based polymeric formulations and further processed by DLP-3D printing. The fabricated devices detected basic species in aqueous and vapor media, expanding the conventional capabilities of pH indicators. Additionally, the developed material proved to be active also in organic liquid solutions, opening up new and broader applications beyond pH definition. Lastly, stimuli-responsive 3D devices were fabricated and built as a proof of concept, obtaining base-sensitive microfluidics or lab ware.

Experimental

Materials

All reagents and solvents for the synthesis were purchased from Sigma-Aldrich, Merck, Fluka, Riedel de Haen, and Alfa Aesar and used without further purification unless otherwise noted. All solvents were purchased from VWR, Carlo Erba, and Sigma-Aldrich and used without other purification. The photocurable monomers poly(ethylene glycol) diacrylate (PEGDA) average M_n 250, 575, 700, 1,6-hexanediol diacrylate (M_w 226.27, HDDA), bisphenol A ethoxylate (2 EO/phenol) diacrylate (M_w 572, BEDA), bisphenol A ethoxylate (15 EO/phenol) dimethacrylate (M_w 1700, BEMA), the photoinitiator 2-hydroxy-2-methylpropiophenone, the UV adsorber 2-(2-hydroxy-5-methylphenyl)benzotriazole were obtained from Sigma Aldrich and used as received. Ammonia solution 25%, 1,8-diazabicyclo [5.4.0]undec-7-ene 98% (DBU), dimethyl sulfoxide (DMSO), ethylene glycol, toluene, acetonitrile, propylene carbonate, *n*-hexane, *N*,*N*-dimethylformamide (DMF), acetone, isopropanol, ethanol were purchased from Sigma Aldrich and used as received.

Dye synthesis

The synthetical pathway and all reagents and yields are reported in Scheme 1.

Synthesis of 2,6-dibromo-1,4,5,8-naphthalenetetracarboxylic dianhydride (2)

Compound **2** was prepared following the same procedure reported by Berezin *et al.*[24] The chemical characterization is in agreement with the reported data.

Synthesis of 4,9-dibromo-2,7-dioctylbenzo[*lmn*][3,8] phenanthroline-1,3,6,8 (2*H*,7*H*)-tetraone (3)

Compound **3** was synthesized following the same procedure reported by Modarelli *et al.*[25] The chemical characterization is in agreement with the reported data.

Synthesis of 4,9-bis(allyloxy)-2,7-dioctylbenzo[*lmn*][3,8] phenanthroline-1,3,6,8 (2*H*,7*H*)-tetraone (4)

A freshly prepared solution of AllylONa in allyl alcohol (240 μL of a solution 1 M of NaH in allyl alcohol) was added dropwise

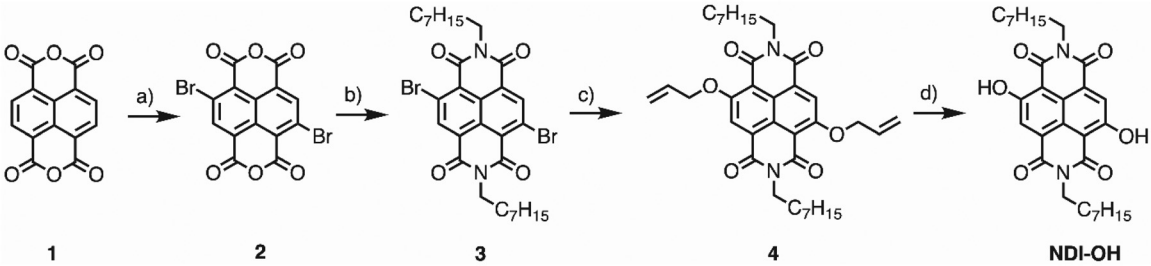

Scheme 1 (a) DBHMH, H_2SO_4, 16 h, 60 °C (b) *n*-octylamine, AcOH, 90 °C, 4 h (64%). (c) AllylONa, DCM, rt, 12 h (28%). (d) Ph_3SiH, $Pd(PPh_3)_4$, DCM, rt, 10 h (56%).

to a solution of **3** (50 mg, 0.08 mmol) in dry CH_2Cl_2 (8 mL). The mixture was stirred at rt for 7 h. Then, CH_2Cl_2 was added, and the organic layer was washed with brine and water, dried over Na_2SO_4 and concentrated *in vacuo*. The crude was purified by flash chromatography (CH_2Cl_2/*n*-hexane 3 : 2), affording **4** as a yellow solid (13 mg, 28%). ^{1}H-NMR (600 MHz, $CDCl_3$): 8.47 (s, 2H), 6.18 (ddt, ^3J(H,H) = 17.2, 10.6, 5.2 Hz, 2H), 5.72 (dq, ^3J(H,H) = 17.2 Hz, ^2J(H,H) = 1.2 Hz, ^4J(H,H) = 1.4 Hz, 2H), 5.45 (dq, ^3J(H,H) = 10.6 Hz, ^2J(H,H) = 1.2 Hz, ^4J(H,H) = 1.4 Hz, 2H), 5.02 (dt, ^3J(H,H) = 5 Hz, ^4J(H,H) = 1.5 Hz, 4H), 4.15 (t, ^3J(H,H) = 7.8 Hz, 4H), 1.73 (qt, ^3J(H,H) = 7.8 Hz, 4H), 1.42 (qt, ^3J(H,H) = 7.7 Hz, 4H), 1.36 (qt, ^3J(H,H) = 7.6 Hz, 4 H), 1.32–1.25 (m, 12 H), 0.87 (t, ^3J(H,H) = 6.8 Hz, 6H). ^{13}C-NMR (150 MHz, $CDCl_3$): δ 162.53, 161.27, 159.80, 131.60, 127.80, 123.88, 120.12, 119.47, 111.36, 71.61, 43.44, 31.96, 29.46, 29.36, 28.14, 27.31, 22.79, 14.79.

Synthesis of 4,9-dihydroxy-2,7-dioctylbenzo[*lmn*][3,8] phenanthroline-1,3,6,8 (2*H*,7*H*)-tetraone (NDI-OH)

To a solution of **4** (13 mg, 0.02 mmol) and $Pd(PPh_3)_4$ (1.3 mg, 0.001 mmol) in dry CH_2Cl_2 (3 mL), phenylsylane (17.3 mg, 0.16 mmol) was added. The mixture was stirred under Argon at rt for 12 h. Volatiles were removed *in vacuo*, and the reaction crude was purified by flash chromatography (CH_2Cl_2/*n*-hexane 1 : 1), affording **NDI-OH** as a yellow solid (6 mg, 53%).^{1}H-NMR (600 MHz, $CDCl_3$): 12.38 (s, 2H), 8.30 (s, 2H), 4.17 (t, ^3J(H,H) = 7.7 Hz, 4H), 1.73 (qt, ^3J(H,H) = 7.6 Hz, 4H), 1.42 (qt, ^3J(H,H) = 7.6 Hz, 4H), 1.36 (qt, ^3J(H,H) = 7.4 Hz, 4 H), 1.32–1.25 (m, 12 H), 0.87 (t, ^3J(H,H) = 6.9 Hz, 6H). ^{13}C-NMR (150 MHz, $CDCl_3$): δ 168.55, 166.42, 161.92, 160.68, 127.25, 123.94, 106.96, 40.75, 31.93, 29.38, 29.32, 28.09, 27.19, 22.77, 14.24.

3D printable formulation

The photocurable formulations (Table 1) were prepared by first dispersing the photoinitiator in liquid monomers and then adding the UV adsorber or the dye. The dye is added as a powder or previously dispersed in acetone to increase its solubility. The formulations obtained are mixed by sonication and, in the required cases, placed at 50 °C until complete evaporation of the added solvent.

Characterization

Nuclear magnetic resonance ^{1}H NMR (600 MHz) and ^{13}C NMR (151 MHz) experiments were conducted using a JEOL ECZ-R instrument (^{1}H operating frequency 600 MHz).

Preliminary analyses were conducted to determine the most suitable polymeric matrix for the desired application. Formulations #1 to #6 (Table 1) were used to prepare samples.

Some preliminary samples were prepared as follows. Ten formulations' drops spread on glass were photopolymerized by irradiating with the UV lamp Hamamatsu LC8 (time: 5 s; UV-light intensity: 5.3 mW cm^{-2}) in a nitrogen atmosphere. The samples were used to evaluate the materials' behavior after 1 hour of direct contact tests (by soaking the samples into the

Table 1 Composition of the photocurable formulations

Identifying name	Monomeric resin	Photo-initiator (phr)	UV Adsorber (phr)	NDI-OH		Sonication time	Solvent evaporation at 50 °C
				phr	Physical state[a]		
#1	PEGDA 250	2.5	—	0.1	P	60 min	—
#2	PEGDA 575	2.5	—	0.1	P	60 min	—
#3	PEGDA 700	2.5	—	0.1	P	60 min	—
#4	HDDA	2.5	—	0.1	P	60 min	—
#5	BEDA	2.5	—	0.1	P	60 min	—
#6	BEMA	2.5	—	0.1	D1	15 min	—
B_NDI-OH	BEMA	2.5	—	0.1	D5	15 min	Yes
P575_NDI-OH	PEGDA 575	2.5	—	0.1	D5	15 min	Yes
P575_UV	PEGDA 575	2.5	0.2	—	—	15 min	—
P575	PEGDA 575	2.5	—	—	—	15 min	—

[a] P: dye is added as powder, D1: dye previously dispersed in acetone (1 mg ml^{-1}), D5: dye previously dispersed in acetone (5 mg ml^{-1}).

solution) and indirect contact (by exposing the samples to the solutions' vapors) with a water/ammonia solution (ammonia concentration of 25% by weight, $pH_{(25\ °C)} > 12$).

For the indirect contact test, the samples were inserted in a closed system together with a solution vat and kept at 37 °C to promote evaporation. Direct contact test was carried out also on P575_NDI-OH and B_NDI-OH DLP-3D printed samples.

Real-time rheological measurements were performed using an Anton Paar rheometer (Physica MCR 302) in parallel-plate mode with a Hamamatsu LC8 lamp equipped with an 8 mm light guide, with a bulb emitting UV light. The measurements were conducted using a quartz window and two set-ups characterized by different light intensities: 0.5 and 4.7 mW cm^{-2} (evaluated on the quartz window). The gap between the two plates was set to 0.2 mm; the samples were kept at a constant temperature (25 °C) and under a constant shear frequency of 10 rad s^{-1}; the light was turned on after 1 min to stabilize the system. The variation of storage (G') and loss (G'') shear moduli during irradiation was measured as a function of exposure time. The measurements were carried out in the linear viscoelastic region (LVE) with a strain amplitude of 0.3%. The LVE was previously evaluated by performing an amplitude sweep measurement at 10 rad s^{-1} (strain from 0.1 to 100%).

An Asiga MAX UVX27 DLP-3D printer (build area: 51.8 × 29.2 × 75 mm^3, light emission at λ = 385 nm, nominal *XY*-pixel resolution of 27 μm, layer thickness adjustable from 1 to 500 μm) was used to print all the samples. The light intensity, the exposure time, and the layer thickness were optimized for each material and the 3D model to be printed (Tables S1 and S2†). The build platform was covered with a glass layer to improve the optical quality of the sample's surface. After the printing process, a 3 minutes post-curing step was performed in a UV oven equipped with a medium-pressure mercury lamp provided by Robot Factory (UV-light intensity 12 mW cm^{-2}).

Printing fidelity to the original CAD models was evaluated through a 3D optical scanner (E4, 3Shape, sensitivity 4 μm) by comparing the scanned data and the reference model. Results are displayed as a colored 3D map of the geometrical deviation from the original cad model.

Fourier Transform Infrared Spectroscopy (FTIR-ATR) tests were performed with a Nicolet iS50 FTIR Spectrometer using the Attenuated Total Reflection mode (32 scans from 400 to 4000 cm^{-1}, resolution of 4.0 cm^{-1}). The cross-linking process was evaluated by monitoring the disappearance of the peak at 810 cm^{-1} (related to the C–H bond stretching in the acrylic group) compared to the peak at 1720–1730 cm^{-1} (C═O bond stretching in the acrylic group). The conversion degree (CD%) was calculated by eqn (1):

$$CD\% = \left(1 - \frac{A_{\text{cross-linked}}}{A_{\text{formulation}}}\right) \times 100 \quad (1)$$

where A is the ratio between the underlying area under the peak at 810 cm^{-1} and 1720–1730 cm^{-1}. FTIR-ATR tests were performed both on the surface (before and after post-curing) and in the core of the material (cut sample), to evaluate the difference of conversions in bulky structures.

After printing and post-curing steps, gel content tests were performed to evaluate the cross-linked fraction (insoluble fraction) and the residual unreacted monomers. The samples were held in a net, weighted, and soaked in two solvents (water and chloroform) for 24 hours. Then, the samples were dried until no mass variation was detected. The gel content (GC%) was evaluated as reported in eqn (2):

$$GC\% = \frac{m_{\text{dried}}}{m_0} \times 100 \quad (2)$$

where m_0 is the initial sample's mass, while m_{dried} is the sample's residual mass after the solvent extraction.

Dynamic-mechanical analyses (DMA) were conducted on a Triton Technology DMA (Mettler-Toledo) in a tensile configuration (frequency: 1 Hz, temperature: from −50 to 30 °C, heating rate: 3 °C min^{-1}, sample length: 10.35 mm, strain amplitude: 0.2 mm).

Water vapor permeability analyses were conducted on 3D-printed specimens (thickness 0.60 ± 0.02 mm, surface area: 2.01 cm^2) with an EXTRASOLUTION MultiPerm (temperature: 25.0 °C, RH: 100%; pressure: 1 bar, gas flow: 12.2 ml min^{-1}). Permeability was calculated by eqn (3):

$$P = \frac{\text{WTR} \cdot l}{p} \quad (3)$$

where WTR is the water transmission rate plateau, l is the sample thickness, and p is the pressure.

UV-Visible absorbance spectra were collected to evaluate the color responsivity towards acid or basic vapors and liquid through the BioTek Synergy HTX Multi-Mode Reader (wavelength: 300–700 nm, sensitivity: 5 nm). P575_NDI-OH samples' data were normalized for the absorbance value at 460 nm; instead, for solutions and P575 samples, the curves were multiplied for a scaling factor (for more details, see eqn (S1) and (S2) in the ESI†).

Those analyses were employed to detect the material colorimetric responsivity to bases and the process' kinetics and reversibility (the conditions are reported in Tables S3 and S4†). For the pH responsivity, ammonia/water solutions at different concentrations were employed. As organic basis, DBU dissolved in *n*-hexane at different concentrations was employed. In this last case, tests were carried out only in the liquid phase (direct contact test) as DBU has limited volatility ($Ps_{(37.7\ °C)\ DBU}$ = 0.071 bar *vs.* $Ps_{(21\ °C)\ NH_3}$ = 8.866 bar, from compound datasheet).[26,27] Process reversibility was studied by employing HCl/water (for test in vapor and liquid phase) and benzoic acid/*n*-hexane (for test in liquid phase) solutions and monitoring the absorbance spectra evolution of the samples while exposed to air for one month.

Swelling tests were carried out by soaking the samples for 8 hours and measuring the samples' thickness before and after. The swelling degree was calculated by eqn (4).

$$\text{Swelling}\,(\%) = \frac{t_f - t_i}{t_i} \times 100 \quad (4)$$

where t_i and t_f are the initial and final samples' thicknesses.

A smart lid and a fluidic device were 3D printed as a proof of concept. The smart lid was tested under basic vapors from the reaction reported in formula (1), and the color change was video recorded.

Different solutions of DBU in *n*-hexane were used to feed the fluidic through a syringe pump in 4 different tests conducted consecutively on the same device (the concentrations of all employed solutions are reported in Table S5†). Color change obtained in test b and c (Table S5†) was video recorded.

$$Ca(OH)_2 + 2NH_4Cl \xrightarrow{80\,^\circ C} 2NH_3 + CaCl_2 + H_2O \quad (1)$$

Results and discussion

The NDI-OH dye has been prepared by adapting a reported procedure (see Scheme 1 and the Material and methods section for the synthetic details). Then, the optical properties were evaluated by dissolving the NDI-OH in chloroform and adding an organic base (DBU) to induce deprotonation of one or both OH groups in the NDI core (species in Fig. 1a). As depicted in Fig. 1b, increasing the concentration of DBU, the maximum in the absorbance spectrum of NDI-OH can be shifted from 464 nm (yellow line) toward 565 nm (red line), and finally, when both OH groups are deprotonated to 605 nm (blue line). Complete photophysical characterization in different solvents is reported in the ESI (Fig. S1†). Preliminary tests were carried out to select the most suitable monomers to develop the 3D printable formulation. Here, four aspects should be taken into account: (i) highly printable monomers should be preferred to facilitate the 3D printing process; this includes viscosity in a suitable range and high photopolymerization reactivity;[11,28] (ii) it is preferred to have good miscibility between monomers and dyes, avoiding the use of solvents that should be then removed;[11,29] (iii) once cured, the polymeric matrix should be permeable to aqueous vapors, to facilitate contact with bases and let the color change process takes place;[21] (iv) the polymeric matrix should trap the dye, avoiding leakage during use.

Starting from these considerations, six polymeric resins were tested, and among those, PEGDA 575 was selected for further

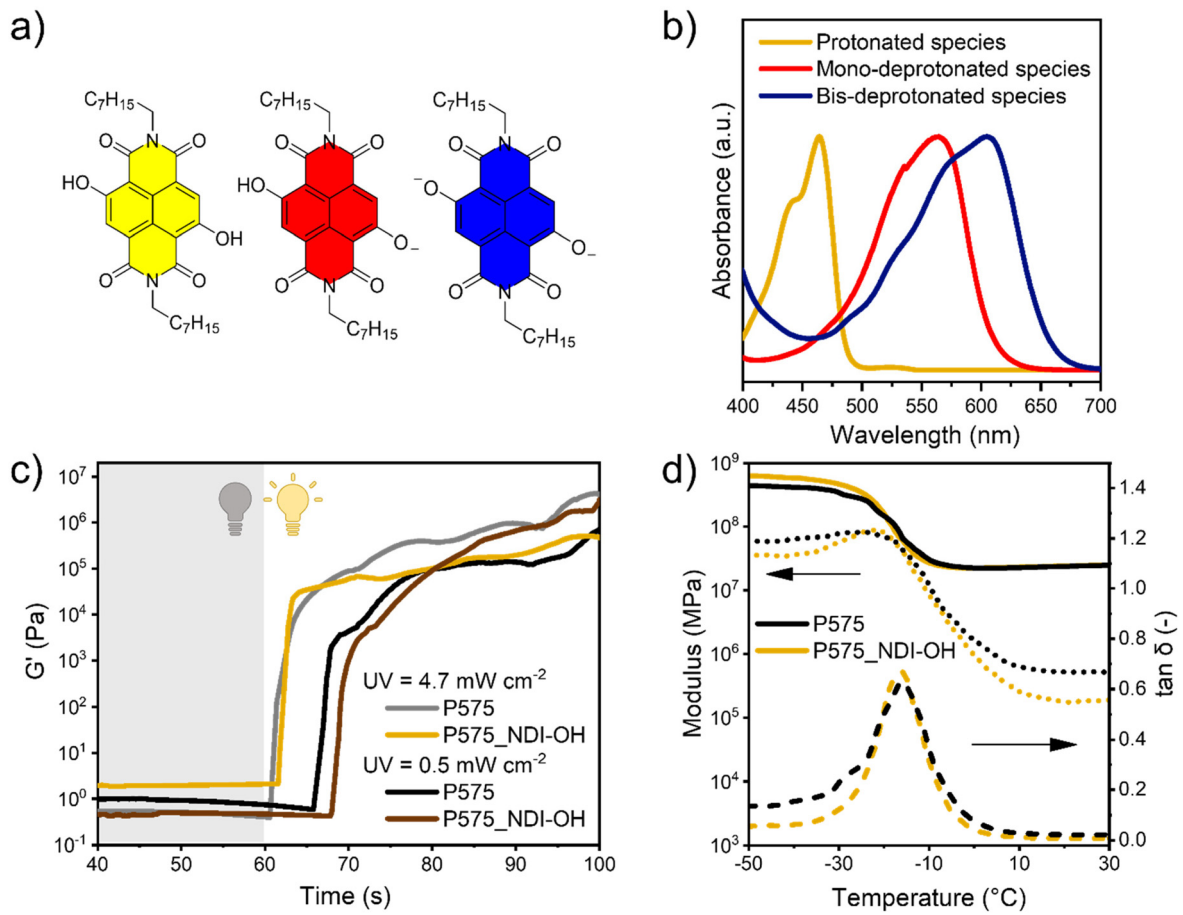

Fig. 1 (a) Protonated and deprotonated species of the NDI OH molecule; (b) absorption spectra of NDI OH in chloroform with increasing DBU concentration; (c) evolution of P575 and P575_NDI OH storage moduli (*G*′) during UV-light irradiation (light switched on after 60 s); (d) DMA plots of P575 (black) and P575_NDI OH (orange) samples. Storage modulus (*E*′) solid line; Loss modulus (*E*″) dotted line, tan δ dashed line.

experiments. A detailed explanation of the rationale beyond these choices and preliminary experimental results are reported in the ESI (Fig. S2, S3,† and in the descriptive paragraph).

Afterward, the cross-linking process of the P575/NDI-OH system was studied through a photorheological analysis of P575 and P575_NDI-OH formulations (Fig. 1c). Even if the presence of the dye competes in the light absorption with the photoinitiator (Fig. S4†), photorheology results indicate that the presence of NDI-OH (in the low amount employed of 0.1 phr) does not affect polymerization or slower the process kinetics.

In both formulations, the polymerization occurs rapidly (around 1 s under 4.7 mW cm^{-2} UV light irradiation), and the curves are almost superimposable, suggesting that the dye does not affect the kinetics in these conditions. Even decreasing the light intensity one order of magnitude (0.5 mW cm^{-2}), the curves are similar despite the expected delay in the start of the polymerization.

Photorheological analysis cannot be directly translated into the parameterization of the printing process, as the measurement conditions and the light source used are different. However, it gives valuable indications for their setting, creating a data set that must be optimized directly during the printing steps.

The printing parameters were optimized to reach satisfactory printing fidelity to the CAD models and a high printing resolution. The parameters (see Tables S1 and S2†) are the same for both formulations.

During the optimization process, two complex geometries were selected: the honeycomb depicted in Fig. 2a, which shows a complex geometry on the *XY* plane, and the hollow cube (Fig. S5a†) to test the resolution along the *Z*-axis.

The resolution and the printing fidelity reached with the two samples (Fig. 2b and Fig. S5b†) were evaluated employing a 3D scanner. The scanned model is compared to the original one, resulting in a heat map that describes the geometrical deviation between the models, shown in Fig. 2c for the honeycomb and Fig. S5c† for the hollow cube. The standard deviation between positive and negative displacements of the honeycomb model is equal to ±0.12 mm. This result is improved by the hollow cube sample, reaching a standard deviation of ±0.11 mm. Those data indicate excellent printing fidelity, even if some minor defects of uncontrolled polymerization can still be observed in hanging structures (see Fig. S5c†). These data demonstrated that the formulation containing the NDI-OH dye could be 3D printed, obtaining satisfactory resolutions even for samples with complex geometries.

Conversion degrees of double bonds were measured by ATR in both P575 and P575_NDI-OH samples (Table 2 and ATR measurement in Fig. S6 and S7†), obtaining similar results in both the samples. As expected, conversion was measured slightly higher on the surface than in the bulk of materials, due to different light irradiation of the post-curing process. Nevertheless, all these measurements agree with photorheology results, demonstrating that the presence of NDI-OH slightly influences the polymerization kinetics during the 3D printing process. This is also confirmed by the gel extraction tests performed in water and chloroform, which showed very high values (>90%) of insoluble fraction (Table 2). On the other hand, since gel content was not 100%, it is possible to argue that dye can be leached during this process, so an evaluation of its possible leaching was conducted after the gel content tests, noticing no evidence of dissolved dye (Fig. S8†). This suggests that the extracted part can be related to unreacted monomers or errors in weight measurements. Nevertheless, those values are compatible with the values of fully cured materials. As expected, considering the low

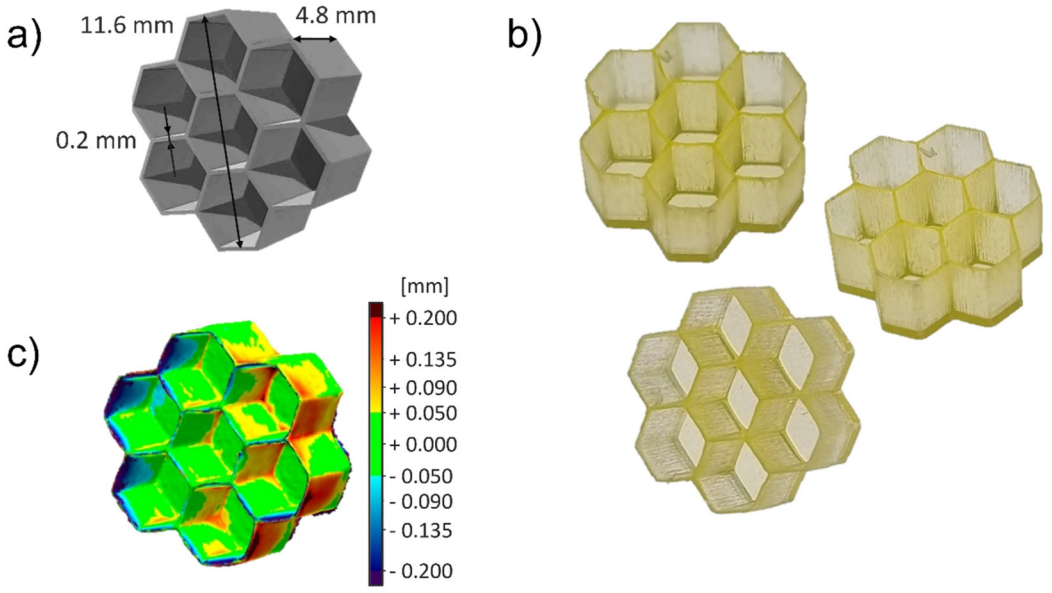

Fig. 2 (a) Honeycomb CAD model; (b) pictures of P575_NDI-OH 3D printed sample with honeycomb geometry; (c) printing fidelity heat map obtained comparing 3D-scanned model and the original CAD model.

Table 2 Gel content test results, conversion degree, and DMA of P575 and P575_NDI OH samples

		Gel content		Conversion degree		DMA	
		In water (%)	In chloroform (%)	Surface (%)	Core (%)	E'^{a} (MPa)	T_g (°C)
P575	After 3D printing	—	—	96	—	—	—
	After post-crosslinking	97.0	91.1	99	81	25	−16
P575_NDI-OH	After 3D printing	—	—	85	—	—	—
	After post-crosslinking	95.1	90.0	94	82	25	−16

[a] Evaluated at 25 °C.

amount of dye, DMA analysis confirmed that NDI-OH presence does not affect thermomechanical properties (Fig. 1d and Table 2).

After the polymeric characterization, some investigations were conducted to evaluate the material's behavior in contact with aqueous vapors and liquid organic phases, to verify the material's compatibility with possible final applications.[30–32]

In this context, the thickness of the sensing material is crucial since very thin specimens have a faster response due to rapid diffusion processes, but low mechanical properties.[20] For this reason, a trade-off value of 0.5 mm was set (see ESI file and Fig. S9†). Regarding the water, the permeability test showed a good affinity with vapor (Fig. S10 and Table S6†) and no visible damages were produced even after 18 hours of contact. The promising results obtained with water vapors are related to resin's hygroscopicity, which on the other hand, leads to some drawbacks for direct contact with liquid water. In fact, both P575 and P575_NDI-OH samples undergo cracking and failure after a prolonged soak in water. For these reasons, the materials developed demonstrated to be more promising as vapor pH sensors than for aqueous solutions. Regarding the material's behavior in organic solutions, *n*-hexane was demonstrated to be the most suitable organic solvent (solvent selection is reported in Table S7†).

The responses of 3D printed materials towards basic agents both in liquid and vapor phases were tested. As mentioned above, NDI-OH gives two distinct color changes at different pH conditions (Fig. 1a). In preliminary tests, it was assessed that this also occurs when embedded in a polymeric matrix, directly and indirectly in contact with NH_3 solutions (Fig. S2†).

Nevertheless, in view to develop functional devices, it is necessary to define in detail the response and kinetics of the 3D printed materials in different conditions by UV-visible spectroscopy. Negative controls performed on the neat P575 samples confirmed that there are no changes in absorption in

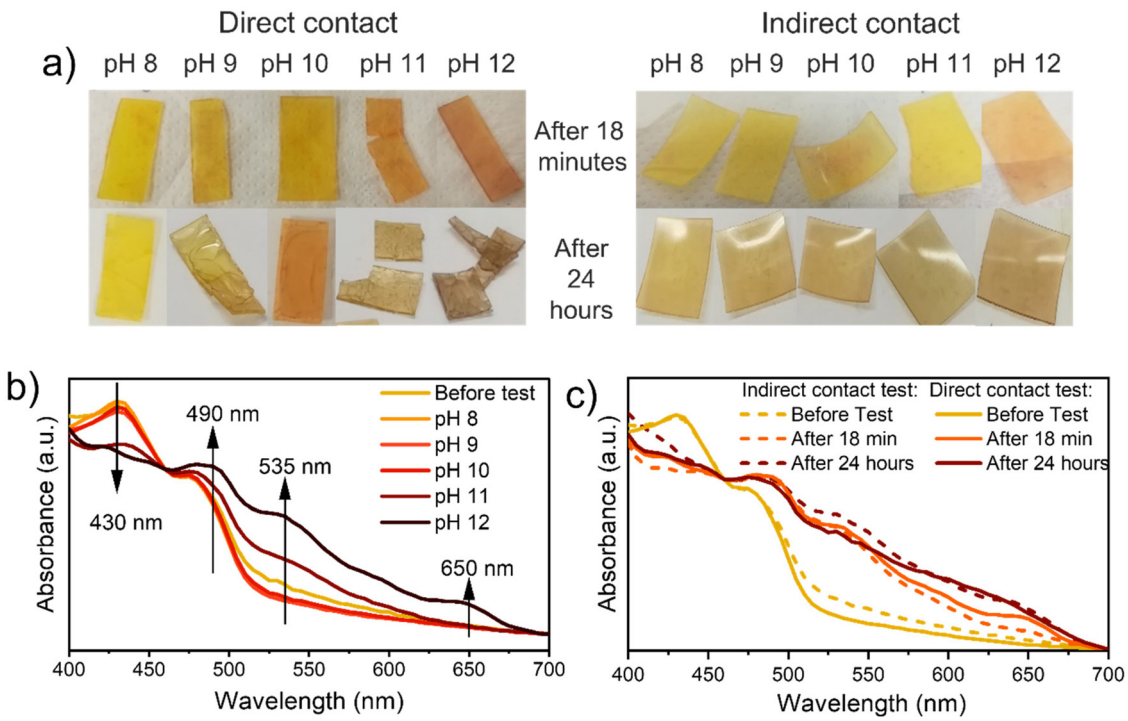

Fig. 3 (a) Pictures of P575_NDI-OH samples after 18 minutes or 24 hours of direct and indirect contact test with NH_3/H_2O solutions at different pH; (b) visible absorption spectra of P575_NDI-OH samples tested for 18 minutes by direct contact with NH_3/H_2O solutions at different pH; (c) comparison between the absorption spectra of P575_NDI-OH samples tested at pH 12 for 18 minutes and 24 hours by direct and indirect contact test.

basic conditions (Fig. S11, and S12†). Similarly, the P575_NDI-OH doesn't show any color change when in contact with water and *n*-hexane (Fig. S8, and S11†).

Afterward, colorimetric analyses were conducted by testing the samples both *via* direct and indirect contact with ammonia solutions. For those analyses, ammonia was selected as a base because, thanks to its high volatility, it is suitable for the indirect contact analyses set-up.

Increasing the solutions' pH, all samples turn from yellow to red/brown (Fig. 3a). The variation of visible light absorption is reported in Fig. 3b after 18 minutes of direct contact with ammonia solution at different pH, while variation after 24 hours and indirect contact test results are reported in Fig. S13.† In all conditions, the peak involved in the absorbance variation are at (i) 430 nm, (ii) 490, (iii) 535 nm, (iv) 650 nm. The first one decreases by increasing the solution pH since it is related to the absorbance of the protonated NDI-OH species (yellow). The others, instead, increase by increasing the pH, since those are related to the absorbance of the red mono-deprotonated (490 and 535 nm) and blue bis-deprotonated NDI-OH species (650 nm) respectively. The time dependency and the comparison between liquid and vapor exposure at pH 12 can be observed in Fig. 3c, which evidences the strong similarity between the color evolution through 24 hours in these two experiments. As shown in Fig. 3c media's physical state doesn't affect the final NDI-OH color nor process kinetics in the chosen matrix. More interestingly, also DBU solutions in *n*-hexane cause a color variation from yellow to magenta

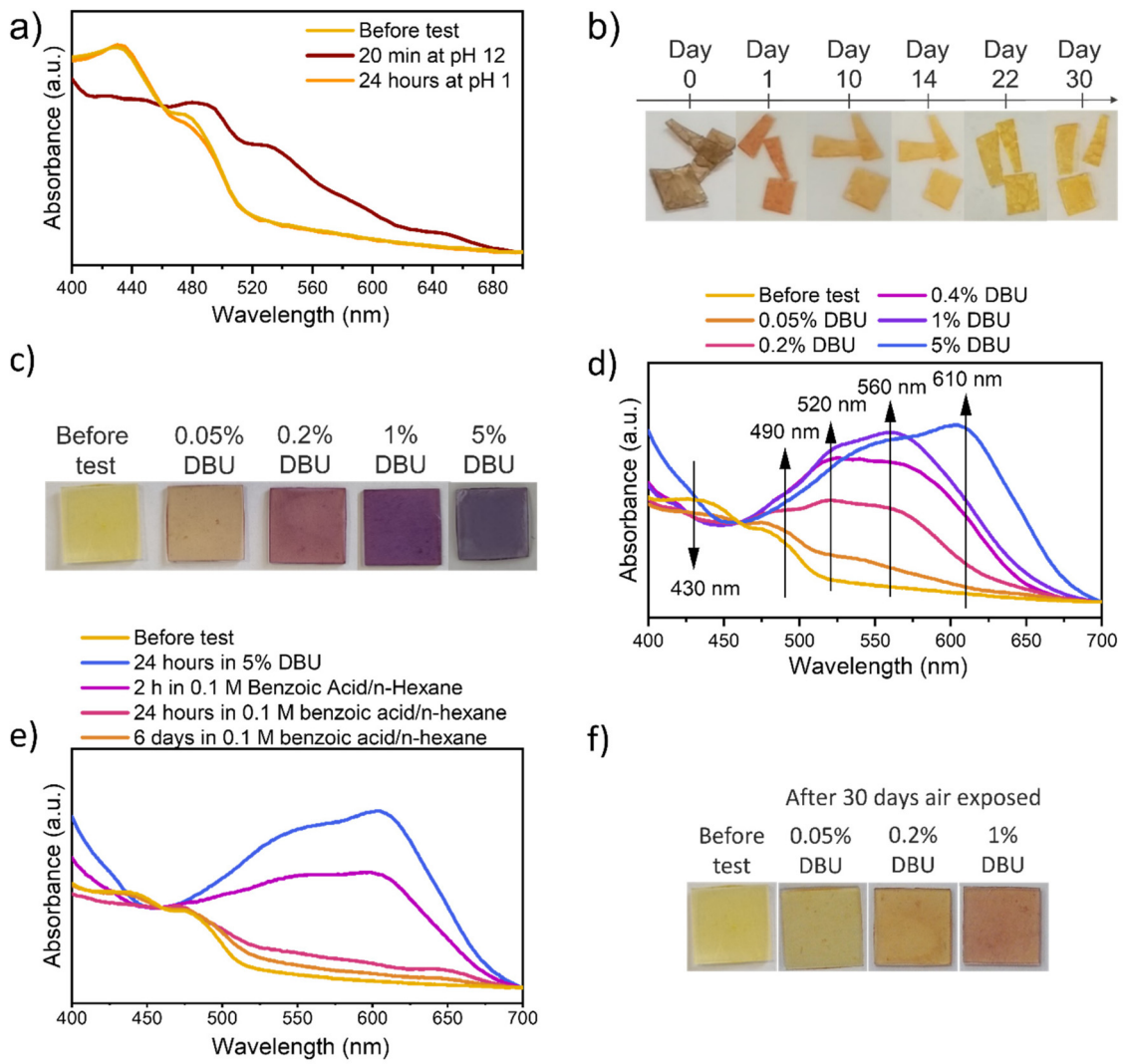

Fig. 4 (a) Visible absorption spectra of a P575_NDI-OH sample previously soaked in liquid NH_3/H_2O solutions at pH 12 and then in HCl/H_2O at pH 1; (b) color evolution of a P575_NDI-OH sample previously soaked for 24 hours in liquid NH_3/H_2O at pH 12 and then exposed to air; (c) pictures and (d) visible absorption spectra of P575_NDI-OH samples tested for 24 hours in liquid solutions of DBU/*n*-hexane with different concentrations; (e) visible absorption spectra of a P575_NDI-OH sample previously soaked for 24 hours in 5% DBU/*n*-hexane solutions and then in 0.1 M benzoic acid/*n*-hexane solution; (f) color evolution of a P575_NDI-OH sample previously tested for 24 hours in DBU/*n*-hexane solutions with increasing DBU concentration and then exposed to air for 30 days.

and finally to blue, as shown in Fig. 4c. The involved wavelength and their trends (Fig. 4d) are similar to those involved with ammonia solution, except for a little shift towards shorter wavelengths. Compared with ammonia, DBU induces a wider color variation, allowing the sample to reach a blue color. Furthermore, P575_NDI-OH proved to be quite sensitive to the DBU presence: the complete color evolution is observed with concentrations lower than 1%.

Also in this case, process's reversibility was investigated by using acid species. Complete reversibility is reached in 6 days of immersion in 0.1 M benzoic acid/*n*-hexane solution, as shown in Fig. 4e; allegedly, stronger acid or higher concentration will speed up the process. Comparing color evolution while exposing P575_NDI-OH to air in all conditions, it is evident that the requested time strongly depends on the basic agent's absorbed quantity and volatility. In fact, as observed before for samples tested with ammonia solution, air reversibility speeds up by decreasing the sample thickness and the time exposed to basic conditions. This consideration is confirmed by the analysis with DBU, in which increasing DBU concentration in the initial test solution slows down the air reversibility. In fact, after 30 days of air exposure, only the sample tested with 0.05% DBU reached a color similar to the original one (pictures in Fig. 4f and spectra in Fig. S18†).

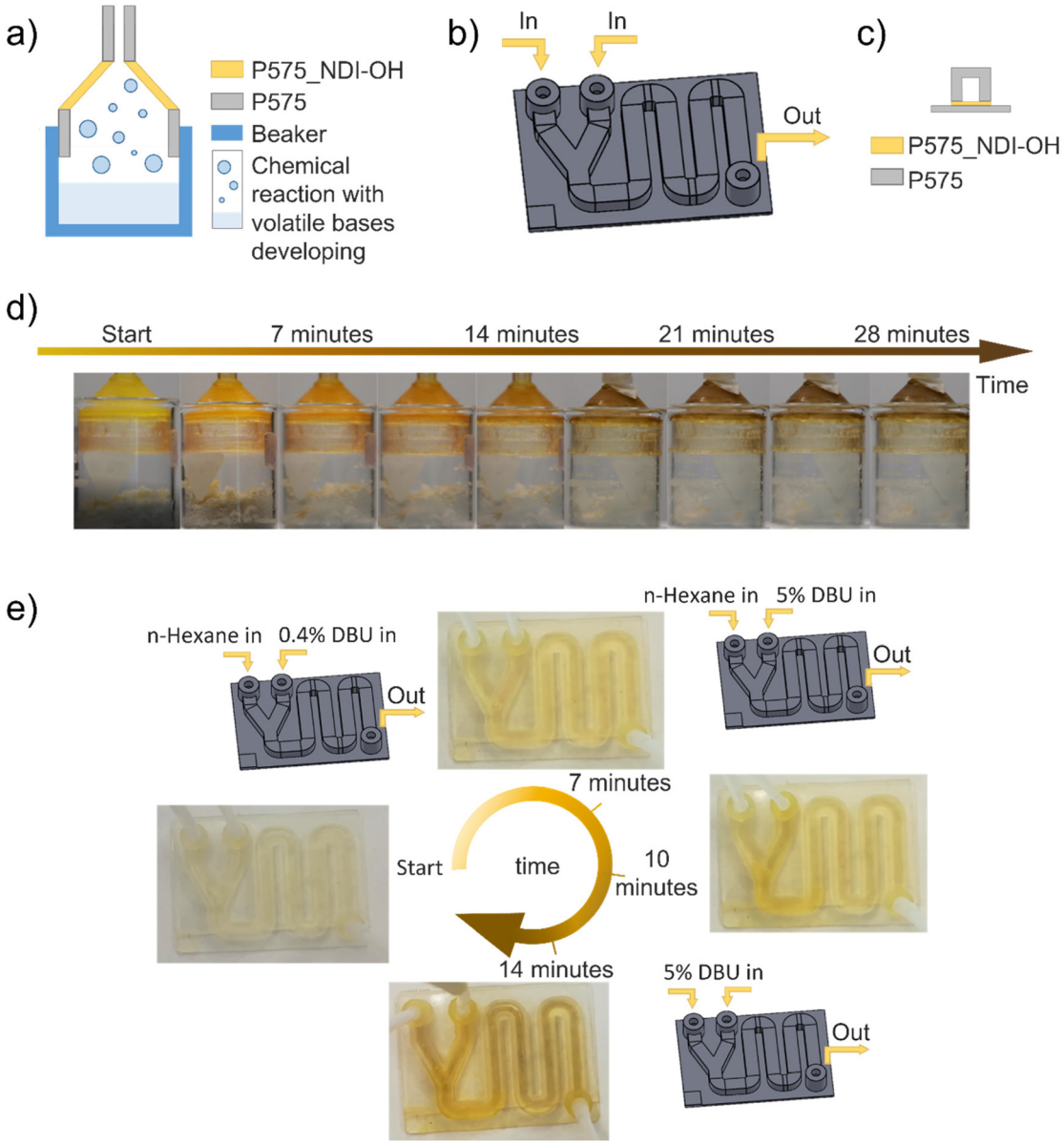

Fig. 5 (a) Schematic representation of the smart lid's composition and application; (b) schematic representation of the fluidic application; (c) schematic representation of a fluidic channel section; (d) smart lid application to monitor the evolution of the reaction reported in formula (1), by sensing the generated vapor; (e) demonstration of the fluidic application by feeding solution with different DBU concentration. Pictures show the final color reached at the end of the tests, drowns are schematic representations of the test feeding solutions.

At last, two functional devices were 3D printed as proof of concept for the potentialities of the developed material. When designing a device, also based on the results here reported, many parameters should be taken into account, in particular: (i) the thicker is the sample, the more evident is the color to a naked-eye; (ii) the thicker is the sample, the slower is the overall color change, since this belongs to diffusion, that is a time-depending process; (iii) the thicker is the sample, the tougher is the part. So, a trade-off must be reached to have clear but fast color change, together with devices easy to manipulate. Because making very thin sample will lead to fast color change but not so visible and, mainly, hard to manipulate. On the contrary, very thick materials may suffer of superimposition of colors, giving a final appearance which is the result of already converted dyes with still unconverted ones.

Starting from these assumptions, two devices were designed to monitor a chemical reaction's progress: the first one is a smart lid that works by sensing basic vapor to detect acid or bases. Instead, the second one is a fluidic that can be used with liquid organic solutions to detect bases. Those devices can be employed as colorimetric sensors, thanks to the presence of P575_NDI-OH in a desired part of the components, *i.e.* funnel part of the lid (0.7 mm thick) and the lower part of the fluidic channel (0.2 mm thick). A schematic representation of their application is reported in Fig. 5a–c.

The fabrication of a multimaterial device along *Z*-axis is a peculiar characteristic of DLP, obtained by changing the printable materials at the desired layer(s). Furthermore, the different materials don't need bonding or other treatments since the distinct layers chemically react by photopolymerization.

The smart lid was employed to detect ammonia molecules in vapor phase released during a chemical reaction (formula (1)). The color evolution of the 3D printed device shown in Fig. 5d and Movie S1† demonstrates the suitability of this approach. Similarly, a 3D-printed fluidic device can monitor a chemical reaction in its channel. For that scope, a reaction containing an organic base (DBU) was simulated in the device, which showed an evident color variation along the path (see Fig. 5e, Movies S2, and S3†). In this frame, it is worth mentioning that reaction time must be comparable with the time needed to complete the channel path, according to the channel length and the volumetric flow rate.

Conclusions

This work successfully developed a DLP 3D printable material to detect basic species, embedding a halochromic dye in polymeric photocurable formulations. The colorimetric response is obtained thanks to the functional dye NDI-OH, synthesized *ad-hoc* for this purpose. The molecule translated its optical properties to the polymeric matrix, allowing to reach high printing resolution and excellent printing fidelity. Among all the tested printable materials, PEGDA 575 was selected since it showed a better response.

P575_NDI-OH was developed as a reversible solid pH indicator for basic sensing, both in the aqueous and vapor phase, even if the developed structures demonstrated to be more suitable for gas-phase sensing since prolonged soaking in water may cause cracking and/or failure. In addition, during this study, the material has proved to work also in organic liquid solutions (*e.g.*, DBU in *n*-hexane), a well-known not-nucleophilic and hindered organic base. Colorimetric response to basic vapors (NH_3) or liquid organic solutions (DBU in *n*-hexane) is very fast, occurring in 6–12 minutes. The process is entirely reversible by employing acid solutions (1–6 days) or exposing the converted sample to air (3–30 days).

The material potentialities are, finally, demonstrated by the 3D printing of two smart lab ware as proof of concept, designed to monitor a chemical reaction's progress. The findings here reported demonstrate the successful development of 3D printed materials with new functionalities, which are a fundamental step forward in the field and towards new applications. Furthermore, the polymeric materials studied can monitor also vapors and organic solutions, which are beyond conventional applications of pH sensitive dyes and related uses. At last, also multimaterial printing was demonstrated, enabling the possibility to fabricate complex devices with distinct functionalities in the different parts.

Author contributions

B. T. Investigation, writing – original draft, M. G. investigation, writing – review & editing, G. R. visualization, C. F. P. resources C. B. resources, writing – review & editing A. F. validation, writing – review & editing I. R. conceptualization, supervision, writing – review & editing.

Conflicts of interest

There are no conflicts to declare.

References

1 Y. Xu, X. Wu, X. Guo, B. Kong, M. Zhang, X. Qian, S. Mi and W. Sun, *Sensors*, 2017, **17**, 1166.
2 T. D. Ngo, A. Kashani, G. Imbalzano, K. T. Q. Nguyen and D. Hui, *Composites, Part B*, 2018, **143**, 172–196.
3 M. Layani, X. Wang and S. Magdassi, *Adv. Mater.*, 2018, **30**, 1706344.
4 B. C. Gross, J. L. Erkal, S. Y. Lockwood, C. Chen and D. M. Spence, *Anal. Chem.*, 2014, **86**, 3240–3253.
5 J. W. Stansbury and M. J. Idacavage, *Dent. Mater.*, 2016, **32**, 54–64.
6 M. P. Lee, G. J. T. Cooper, T. Hinkley, G. M. Gibson, M. J. Padgett and L. Cronin, *Sci. Rep.*, 2015, **5**, 9875.
7 J. J. Martin, B. E. Fiore and R. M. Erb, *Nat. Commun.*, 2015, **6**, 8641.

8 I. Roppolo, A. Chiappone, A. Angelini, S. Stassi, F. Frascella, C. F. Pirri, C. Ricciardi and E. Descrovi, *Mater. Horiz.*, 2017, **4**, 396–401.
9 S. C. Ligon, R. Liska, J. Stampfl, M. Gurr and R. Mülhaupt, *Chem. Rev.*, 2017, **117**, 10212–10290.
10 J. Zhang and P. Xiao, *Polym. Chem.*, 2018, **9**, 1530–1540.
11 Y. Bao, N. Paunović and J. Leroux, *Adv. Funct. Mater.*, 2022, **32**, 2109864.
12 A. Vitale and J. Cabral, *Materials*, 2016, **9**, 760.
13 M. Gastaldi, F. Cardano, M. Zanetti, G. Viscardi, C. Barolo, S. Bordiga, S. Magdassi, A. Fin and I. Roppolo, *ACS Mater. Lett.*, 2021, **3**, 1–17.
14 F. Frascella, G. González, P. Bosch, A. Angelini, A. Chiappone, M. Sangermano, C. F. Pirri and I. Roppolo, *ACS Appl. Mater. Interfaces*, 2018, **10**, 39319–39326.
15 N. Sakai, J. Mareda, E. Vauthey and S. Matile, *Chem. Commun.*, 2010, **46**, 4225.
16 S. V. Bhosale, M. Al Kobaisi, R. W. Jadhav, P. P. Morajkar, L. A. Jones and S. George, *Chem. Soc. Rev.*, 2021, **50**, 9845–9998.
17 A. Fin, I. Petkova, D. A. Doval, N. Sakai, E. Vauthey and S. Matile, *Org. Biomol. Chem.*, 2011, **9**, 8246.
18 M. Al Kobaisi, S. V. Bhosale, K. Latham, A. M. Raynor and S. V. Bhosale, *Chem. Rev.*, 2016, **116**, 11685–11796.
19 G. J. Mohr and H. Müller, *Sens. Actuators, B*, 2015, **206**, 788–793.
20 Z. Li, J. R. Askim and K. S. Suslick, *Chem. Rev.*, 2019, **119**, 231–292.
21 M. K. LaGasse, J. M. Rankin, J. R. Askim and K. S. Suslick, *Sens. Actuators, B*, 2014, **197**, 116–122.
22 T. M. Butler, B. D. MacCraith and C. McDonagh, *J. Non-Cryst. Solids*, 1998, **224**, 249–258.
23 A. Pastore, D. Badocco, S. Bogialli, L. Cappellin and P. Pastore, *Microchem. J.*, 2021, **160**, 105605.
24 A. A. Berezin, A. Sciutto, N. Demitri and D. Bonifazi, *ACS Publications*, 2015, **17**, 1870–1873.
25 H. Shokouhi Mehr, N. C. Romano, R. Altamimi, J. M. Modarelli and D. A. Modarelli, *Dalton Trans.*, 2015, **44**, 3176–3184.
26 Sigma-Aldrich, **https://www.sigmaaldrich.com/IT/en/product/sial/09682**, (accessed December 16, 2022).
27 Sigma-Aldrich, **https://www.sigmaaldrich.com/IT/en/product/aldrich/139009**, (accessed December 16, 2022).
28 M. Caprioli, I. Roppolo, A. Chiappone, L. Larush, C. F. Pirri and S. Magdassi, *Nat. Commun.*, 2021, **12**, 2462.
29 A. J. Guerra, J. Lammel-Lindemann, A. Katko, A. Kleinfehn, C. A. Rodriguez, L. H. Catalani, M. L. Becker, J. Ciurana and D. Dean, *Acta Biomater.*, 2019, **97**, 154–161.
30 L. Zheng, W. Mei, X. Zou, Y. Zhong, Y. Wu, L. Deng, Y. Wang, B. Yang and W. Guo, *J. Org. Chem.*, 2022, **88**, 272–284.
31 I. J. Ochuma, R. P. Fishwick, J. Wood and J. M. Winterbottom, *Appl. Catal., B*, 2007, **73**, 259–268.
32 S. Ghavam, M. Vahdati, I. A. G. Wilson and P. Styring, *Front. Energy Res.*, 2021, **9**, 580808.